RSC Advances

ROYAL SOCIETY OF CHEMISTRY

www.rsc.org/advances

Cite this: DOI: 10.1039/c0xx00000x

www.rsc.org/xxxxxx

ARTICLE TYPE

Electrospun barium titanate/cobalt ferrite composite fibers with improved magnetoelectric performance

Avinash Baji,*[a,b] Yiu-Wing Mai,[a] Rattikorn Yimnirun[c] and Sujitra Unruan[d]

Received (in XXX, XXX) Xth XXXXXXXXX 20XX, Accepted Xth XXXXXXXXX 20XX

DOI: 10.1039/b000000x

In this study, we use a versatile sol-gel based electrospinning technique to fabricate nanostructured barium titanate ($BaTiO_3$)/cobalt ferrite ($CoFe_2O_4$) composite fibers and analyze their magnetoelectric response. Scanning and transmission electron microscopy images indicate that the obtained fibers are composed of fine grains which are self-assembled and arranged. X-ray diffraction (XRD) study of the composite fibers revealed the presence of perovskite and spinel structures corresponding to $BaTiO_3$ and $CoFe_2O_4$ phases, respectively. The magnetic hysteresis loops of the resultant fibers showed that the fibers were ferromagnetic with magnetic coercivity of 650 Oe and saturation magnetization of 31 emu/g. Moreover, the magnetoelectric coefficient developed on the surface of the fibers was measured as a function of the applied external DC magnetic field. A maximum magnetoelectric coefficient of 13.3 $mV.cm^{-1}Oe^{-1}$ was determined for the composite fibers, which is much higher than the commonly reported values for bulk or thin film counterparts. The large magnetoelectric coefficient of the composite fibers was attributed to the nano-sized grains and their arrangement within the fibrous geometry. The intimate contact and the large interfacial area presented by the nanostructures ensured that the composites displayed strong magnetoelectric behavior. Such composite fibers show tremendous potential for magnetic field sensor applications and for magnetoelectric devices.

Introduction

Multiferroic materials with coexistence of two or more ferroic orders such as ferroelectricity, ferromagnetism and ferroelasticity have attracted a great deal of interest due to their potential applications as multifunctional devices[1-7]. In some multiferroic materials, the interaction between the magnetostrictive and ferroelectric phases gives rise to a new effect called the "magnetoelectric (ME)" effect[1-3]. The ME effect makes it possible for the electrical polarization/magnetization within the material to be controlled with the application of external magnetic/electric field[8,9]. This desired mechanism enables a variety of potential applications for ME materials including sensors, transducers, memory devices which can be electrically written and magnetically read, magnetically controlled piezoelectric devices, etc[1,2,8,9].

The numbers of monophasic multiferroic materials that are capable of displaying the ME effect are limited because it is difficult for the electric and magnetic dipoles to coexist at ambient temperatures within the asymmetrical structures[10,11]. Furthermore, the ME effect in monophasic materials is usually very small[12,13]. Hence, many efforts have been directed towards fabrication of two-phase hetero-structures. ME composites consisting of two phases offer greater flexibility, multi-functionality, and higher ME coupling compared to naturally occurring monophasic materials[1,2,13,14]. The ME effect in such composites depends on the magnetic-strain-electrical coupling between the magnetostrictive and ferroelectric phases[1,15]. When a magnetic field is applied, the magnetostrictive phase within the composite induces a strain in terms of a change in dimensions, which in turn transfers the stress to the ferroelectric phase, resulting in an electric polarization[2,3,16]. This strong coupling enables composites capable of large ME coefficients[9]. However, obtaining good interfacial bonding between the phases is a prerequisite for fabricating composites which are capable of displaying significant ME effects[17]. Composites fabricated using conventional techniques, such as sintering, microwave sintering and hot pressing are found to exhibit low ME coefficient due to the presence of micro-cracks, impurity phases, non-ideal interfaces between the phases, defects, and high leakage currents[2,18,19]. To address this issue, recent studies have focused on fabricating nanostructured composites[15,20-22]. It has been demonstrated that the nanometer length scale of the constituent phases within the composites ensures strong interfacial coupling and intimate contact between the phases[15,16,23].

Herein, we report the fabrication of nanostructured composite fibers using a sol-gel enabled electrospinning technique, hitherto unexplored, and demonstrate that these fibers display well-defined ME behavior. Indeed, very few studies[24-26] have explored the magnetoelectric behavior of electrospun fibers. These studies used piezoresponse force microscopy (PFM) to investigate the local magnetoelectric coupling of the fibers. Magnetic domain patterns were obtained in response to external electric fields

imposed on the fibers to confirm the presence of ME coupling. Here, we obtain $BaTiO_3/CoFe_2O_4$ composite fibers using electrospinning enabled techniques and investigate the ME coefficient of the fibers as opposed to using PFM to probe the local ME coupling and estimating their ME coefficient. The ME coefficient values for bulk composite typically vary between 0.19 to 4 $mV.cm^{-1}.Oe^{-1}$ [10]. We demonstrate that electrospinning is not only useful to fabricate $BaTiO_3/CoFe_2O_4$ composite fibers but it can also help achieve composites that display sizeable ME coefficients. $BaTiO_3$ and $CoFe_2O_4$ are chosen in this study as they are individually known to display good ferroelectric and ferromagnetic behaviors, respectively. In the composite fiber form, they combine the electric and magnetic polarizations to exhibit a prominent ME effect. These one-dimensional ME fibers are suitable for many applications, such as microelectric devices, electromagnetic devices and nano-systems among others.

Experimental

$BaTiO_3/CoFe_2O_4$ composite fibers were fabricated using the sol-gel enabled electrospinning technique. For this purpose, $BaTiO_3$ and $CoFe_2O_4$ precursor sol-gel solutions were separately processed before preparing the electrospinning solution. First, $BaTiO_3$ precursor solution referred to as solution A was prepared by dissolving 2.55 g of barium acetate in 6 ml of acetic acid. 2.95 ml of titanium isopropoxide was added to this solution under constant stirring condition. Following this, $CoFe_2O_4$ precursor solution referred to as solution B was prepared by dissolving 2.9 g of $Co(NO_3)_2.6H_2O$ and 8.08 g of $Fe(No_3)_3.9H_2O$ in 10 ml of dimythlformamide (DMF) solution. Solution A and B were added in a ratio in order to obtain a molar ratio of 1:1 between $CoFe_2O_4$ and $BaTiO_3$.

Electrospinning

The solution for electrospinning was prepared by dissolving 3 g of polyvinyl pyrrolidone (PVP) with molecular weight 360,000 in 11 g of DMF/ethanol solvent mixture (1:1 wt/wt). Solution A was added to the PVP solution drop-wise and under constant stirring condition; then, solution B was added drop by drop. The mixture solution was stirred for 24-36 h until a homogenous solution was obtained.

A syringe with a 23-gauge metal needle was used to electrospin the mixture solution. Electrospinning was conducted at 21 kV and the flow rate of the solution was 0.07 mm/min. 15 cm spacing was used between the tip of the needle and the collector surface.

The obtained fibers were initially dried in an oven at 100 °C for 24 h and subsequently transferred to a furnace for thermal annealing. The fibers were heated from ambient temperature to 750 °C. The heating rate was 5 °C/min and the dwelling time at 750 °C was 1 h.

Structural characterization

Microstructures

The morphology of the fibers was analysed using a field emission scanning electron microscope (FESEM, Zeiss ULTRA *plus*). The precursor fibers and the $BaTiO_3/CoFe_2O_4$ fibers obtained after thermal annealing were coated with gold before they were examined using a SEM at an accelerating voltage of 5 kV. Transmission electron microscopy (TEM, Philips CM120 Biofilter) was used to examine the $BaTiO_3/CoFe_2O_4$ fibers.

X-ray diffraction (XRD)

The crystal structures of the fibers were determined from the XRD patterns of the $BaTiO_3/CoFe_2O_4$ fibers. XRD on the $BaTiO_3/CoFe_2O_4$ samples were conducted in reflection mode at ~25 °C using an X-ray diffractometer (XRD Shimadzu S6000) with CuKα radiation (λ=1.54 Å). The 2θ scan was varied between 15° and 70° and the scan speed was set at 1 °/min with 0.02° step size.

Ferromagnetic behavior

Measurements of the room temperature ferromagnetism for $BaTiO_3/CoFe_2O_4$ fibers were recorded using a commercial Quantum Design magnetic property measurement system (MPMS) and physical property measurement system (PPMS). A vibrating sample method was used to obtain the magnetic hysteresis curves. The magnetic field was ramped at ambient temperature (300 K) from 10,000 Gauss to -18,000 Gauss and back to 18,000 Gauss.

Magnetoelectric effect

To measure the ME response, the fibers were first ground and broken into shorter fragments which were then pressed together under a pressure of 130 MPa and sintered at 1100 °C for 1 h to obtain disk shaped specimens. 5 °C/min was used as the heating rate. The ambient temperature ME effect on the sintered disk specimens was determined using the dynamic lock-in technique. The measurement was performed at a constant frequency of 1 kHz and a constant bias AC magnetic field (5 Oe). The ME coefficient of the samples was measured as a function of the DC magnetic field (H_{DC}) and was obtained by dividing the measured output voltage by the magnitude of applied H_{AC} and the thickness of the sample disk.

Results and discussion

Typically, introduction of indirect coupling through strain between the ferroelectric and ferromagnetic phases within the composite ensures that the composite displays a ME effect[5]. Good coupling and optimized ME response in composites can be obtained by controlling the size of the constituent phases and the quality of the interfacial bonding between them[5]. Thus, composite samples with nanostructured constituent phases can display large ME properties since the nanometer length scale of the constituents offers large interfacial area. In this study, we fabricate barium titanate ($BaTiO_3$)/cobalt ferrite ($CoFe_2O_4$) composite fibers using a sol-gel based electrospinning technique. Our results demonstrate that these fibers composed of nanostructured $BaTiO_3$ and $CoFe_2O_4$ grains display well-defined ferromagnetism and ME coefficient.

The surface morphology of as-spun fibers and fibers obtained after thermal annealing is evaluated using SEM. Figures 1A and 1B show such images of as-spun fibers and $BaTiO_3/CoFe_2O_4$ fibers, respectively. The as-spun precursor fibers in Figure 1A show an average fiber diameter of 300 nm with a smooth fibrous

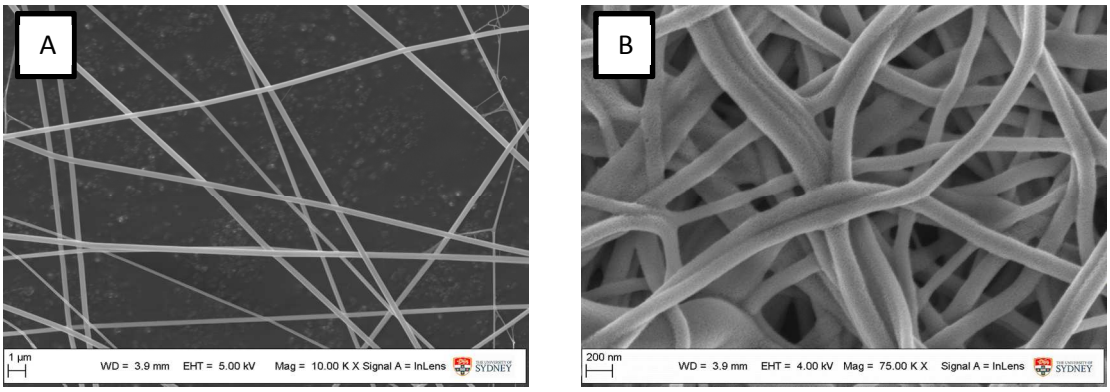

Fig. 1 SEM micrographs of (A) as-spun fibers and (B) thermally annealed $BaTiO_3/CoFe_2O_4$ fibers

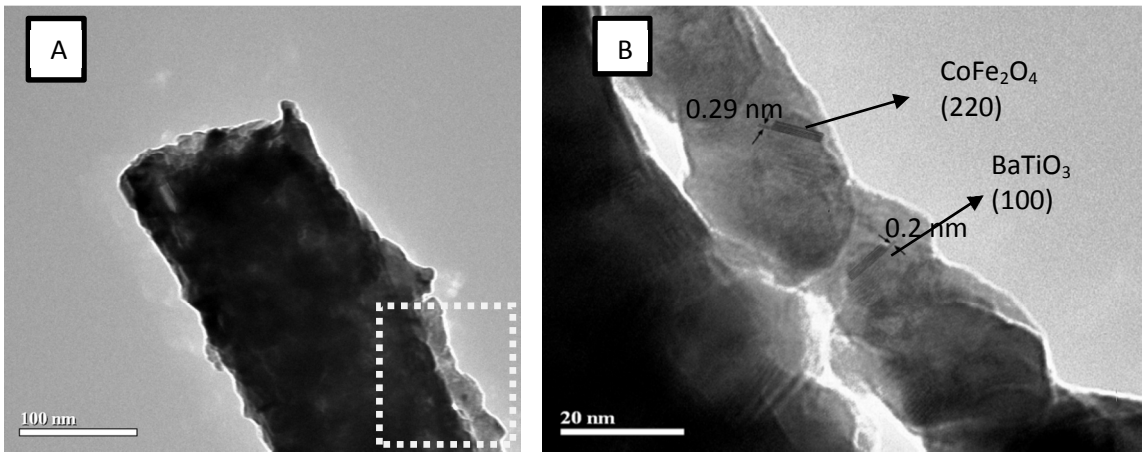

Fig. 2 (A) TEM micrograph of $BaTiO_3/CoFe_2O_4$ composite fiber. (B) High magnification TEM micrograph of a selected region. The image in (B) shows clearly the crystalline lattice structures

morphology. After thermal annealing, brownish black fibers, tens of micrometers in length, are formed. It is clear from Figure 1B that the resultant $BaTiO_3/CoFe_2O_4$ fibers retained their fibrous morphology. However, the diameter of $BaTiO_3/CoFe_2O_4$ fibers is reduced to 140±30 nm, which is attributed to the decomposition of the polymer and crystallization of $BaTiO_3/CoFe_2O_4$.

Figure 2 shows typical TEM images of a $BaTiO_3/CoFe_2O_4$ composite fiber. It is evident that the fiber is composed of fine nanoparticles that are linked and tightly bound. Figure 2B shows that the linked particles display interference of two crystallographic orientations, which originate from the crystals of $BaTiO_3$ and $CoFe_2O_4$. A magnified image using Digital Micrograph software identified the crystallographic phases by measuring the inter-planar spacing, *d*. $BaTiO_3$ is identified by the (100) plane, while $CoFe_2O_4$ the (220) plane. Figure 2B also demonstrates that the $BaTiO_3$ and $CoFe_2O_4$ particles are in close proximity with each other. These results confirm the formation of crystalline $BaTiO_3/CoFe_2O_4$ composite fibers.

X-ray diffraction patterns of the samples are also obtained to confirm the crystalline phases corresponding to $BaTiO_3$ and $CoFe_2O_4$. The XRD patterns of the as-spun precursor fibers (not shown in Figure 3) do not show any peaks, which indicate that the as-spun fibers are amorphous. However, XRD patterns of the thermally annealed sample (Figure 3) shows clear distinct peaks, confirming that the sample is polycrystalline. The diffraction pattern peaks are indexed to the reflections of $BaTiO_3$ and $CoFe_2O_4$ phases[10,20,27]. This illustrates that the $BaTiO_3$ and $CoFe_2O_4$ phase evolution occurs from the amorphous solid phase and during the thermal annealing process. The phases are distinct and appear well segregated. All the reflections can be indexed according to the structures of $BaTiO_3$ and $CoFe_2O_4$[10,11,23]. Thus, it confirms the presence of both perovskite and spinel phases corresponding to $BaTiO_3$ and $CoFe_2O_4$, respectively (JCPDS card number 81-2196 and JCPDS card number 22-1086). The presence of a few unidentified peaks suggests some form of chemical reactions between $BaTiO_3$ and $CoFe_2O_4$ phases during sintering. The peak seen at 37° corresponds to the Co_3O_4 impurity phase (JCPDS card number 42-1467).

Next, we investigate the multiferroic properties of the fabricated composite fibers by measuring their ferromagnetic and direct ME coupling behavior. The magnetic hysteresis loop of the composite fiber measured along the in-plane direction and at room temperature is given in Figure 4 and is typical of magnetic materials[6,15,21,28]. This indicates the existence of an ordered magnetic structure in the fibrous composite. The saturation magnetization of the $BaTiO_3/CoFe_2O_4$ composite fiber is determined from the intercept to the y-axis (magnetization) as 1/H approaches zero. Hence, the saturation magnetization (M_s) of

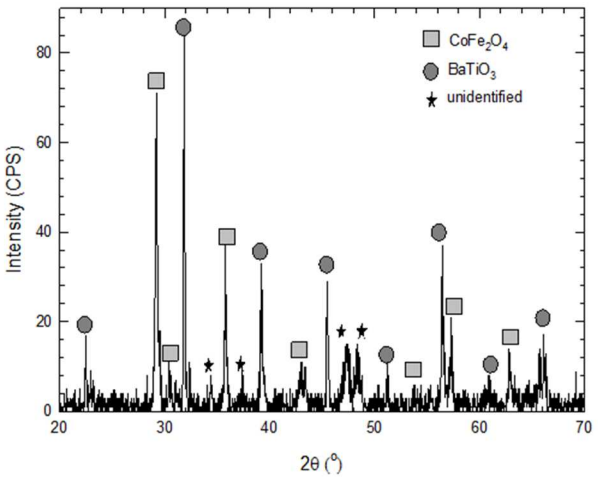

Fig. 3 XRD patterns recorded for $BaTiO_3/CoFe_2O_4$ composite fibers. The XRD peaks clearly indicate the polycrystalline nature of the fabricated fibers. The XRD peaks match closely with the pervoskite and spinel structures corresponding to $BaTiO_3$ and $CoFe_2O_4$ phases, respectively

the sample is ~31 emu/g. It is evident from Figure 4 that the hysteresis loop is asymmetrical about the origin and is displaced to its left. Such displaced hysteresis loops are often seen in composites due to the exchange anisotropy at the ferromagnetic/ anti-ferromagnetic interface[29,30]. The exchange interactions between ferromagnetic and anti-ferromagnetic materials result in the displacement of the hysteresis loops. Our samples are composites consisting of a ferrite phase and a ferroelastic phase. These phases are randomly dispersed within the fiber geometry, causing lattice distortion of the ferrite phase. Hence, the stress generated by this lattice distortion and magnetoelastic coupling between the phases may be responsible for the displaced hysteresis[31]. The presence of the piezoelectric phase within the composite should also play a role in influencing the hysteresis behavior. This is also supported by the results of Rizwan and co-workers[29,30]. They suggest that the coupling between the ferromagnetic and piezoelectric domains and the hindrance to the magnetic ordering of the ferrite phases provided by the ferroelectric phase leads to the asymmetrical hysteresis loops. Study of the exact mechanism responsible for the displaced M-H hysteresis loop is beyond the scope of this work. The coercive field for asymmetric loops can be defined by: $H_C = (H_{c1}-H_{c2})/2$, where H_{c1} and H_{c2} are the right and left coercive fields of the hysteresis loop. Thus, the coercive field is determined to be ~670 Oe. This magnetic coercive field depends on several factors including magneto-crystalline anisotropy, grain size, interface, defects, doping and nature of the surface[23]. The low value of the coercive field recorded at room temperature indicates that the $BaTiO_3/CoFe_2O_4$ composite fibers are magnetically soft and show tremendous potential for device applications[13]. However, the coercive field determined for $BaTiO_3/CoFe_2O_4$ composite fibers is slightly higher than the theoretical coercive field 430 Oe of $CoFe_2O_4$ [32]. We attribute this to the presence of the $BaTiO_3$ phase, which is a non-magnetic phase and makes the magnetization difficult[28].

The saturation magnetization of these composite fibers obtained using the electrospinning technique is found to be higher than the saturation magnetization of some of the ferrite/ferroelectric composite systems reported in[13,27,28]. The higher M_s of our composite fibers can be attributed to the unique processing method. Similar results are obtained by Arias *et al.*[33]. They show that electrospinning leads to elongated grains of the

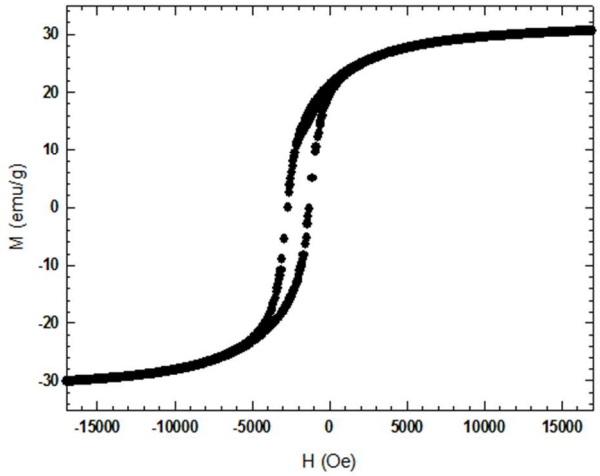

Fig. 4 Magnetic hysteresis loop of $BaTiO_3/CoFe_2O_4$ composite fibers recorded at 300 K. The magnetic hysteresis loop confirms the ferromagnetic behavior of the fibers

ferrite fibers possessing enhanced magnetic properties. These results are well supported by theory, which predicts that fibrous systems having grains arranged and aligned in a linear chain configuration will have their magnetic dipoles also aligned along the fiber axis. The interaction between the dipoles of neighboring grains and the alignment of dipoles contribute towards the enhancement of saturation magnetization[21,33-35]. However, the M_s value for the composite fibers is lower than the theoretical value of 71 emu/g for pure $CoFe_2O_4$ [32] . This is caused by the presence of the non-magnetic $BaTiO_3$ phase within the composite.

Figure 5 shows the dependence of the ME coefficient of the composite fibers on the DC magnetic field. The ME coefficient recorded for the composite fibers is a measure of changes in the electric voltage in response to the applied external magnetic field. During the measurements, a small AC magnetic field (H_{AC}) of 5 Oe is used in conjunction with the DC magnetic field (H_{DC}). It is evident from Figure 5 that the $BaTiO_3/CoFe_2O_4$ composite fibers have a small initial ME coefficient value near zero magnetic bias. At zero magnetic field, the ME coefficient of the composite fibers is ~1.7 $mV.cm^{-1}.Oe^{-1}$. As the magnetic field is increased, the ME coefficient of the composite fibers shows an approximate linear increase with magnetic field and attains a maximum value of 13.3 $mV.cm^{-1}.Oe^{-1}$ at DC magnetic field of ~1810 Oe. At magnetic field greater than 1810 Oe, the ME coefficient value saturates and then decreases with magnetic field. The value (13.3 $mV.cm^{-1}.Oe^{-1}$) at which ME saturates is taken as the ME coefficient of the composite fibers.

Table 1 summarizes the results of some current $CoFe_2O_4/BaTiO_3$ ME composites. Evidently, the ME coefficient we obtained is much larger than those commonly reported on ME coefficient of $BaTiO_3/CoFe_2O_4$ composites prepared from core-shell powder or powder[10,11,36-39] and comparable to those containing nano-lamellar bicrystals[40]. This indicates strong coupling between the ferroelectric ($BaTiO_3$) and ferromagnetic

($CoFe_2O_4$) phases in our fabricated composite fibers. Differences in ME coefficient values reported in the literature may be due to differences in sample characteristics such as constituents, compositions of compounds, sintering temperature, microstructure, size, etc[10,41]. For example, coupling between the phases can be improved by increasing the sintering temperature. However, high sintering temperature can lead to the formation of Fe^{2+} ions in the ferrite phase. These Fe^{2+} ions can reduce the

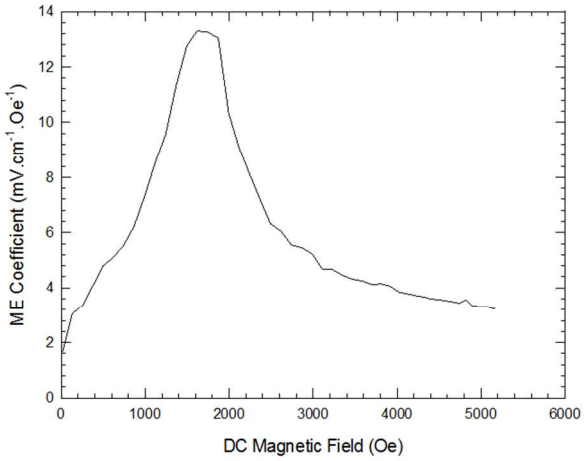

Fig. 5 Dependence of the magnetoelectric (ME) coefficient of $BaTiO_3/CoFe_2O_4$ composite fibers on the DC magnetic field. An AC magnetic field of 5 Oe was applied during the measurements

electrical resistivity of the composite, which is important to achieve a high ME signal[36]. Nie *et al.*[41] reported a high ME coefficient value of ~17 $mV.cm^{-1}.Oe^{-1}$ for their composite particles. They sintered the samples at 1200 °C for 2 h and were able to control the crystallite size of their composite between 35 and 80 nm. Furthermore, their samples were poled before the ME measurements were made. However, low ME values (0.3 to 2 $mV.cm^{-1}.Oe^{-1}$) were also reported in other studies[10,11,38] for similar composites. This could be because of the high sintering temperature and the duration for sintering used for sample preparation. For example, Corral-Flores *et al.*[38] sintered the samples at 1200 °C for 12 h. In addition, the sizes of $BaTiO_3$ and Co_2FeO_4 in the composite were much larger at ~2 μm. These factors could explain the differences in ME coefficient values reported for composite particles in References 41and 38.

Studies which have reported even higher ME coefficient values fabricated composites by dispersing $CoFe_2O_4$ nanorods within the $BaTiO_3$ matrix phase. The dispersion of single crystal nanorods within the $BaTiO_3$ matrix played a role in enhancing the interfacial area between the ferroelectric and ferromagnetic phases and also ensured good ME coupling between these two phases[42,43]. For example, Bai *et al.*[43] reported a ME coefficient of $1.2x10^3$ $mV.cm^{-1}.Oe^{-1}$. Such a high ME coefficient value could be attributed to the large interfacial area obtained by dispersing $CoFe_2O_4$ nanorods within the $BaTiO_3$ phase. Also, the ME coefficient values were obtained using piezoresponse force microscopy (PFM), which only measured the local ME response. $BaTiO_3$ phase was electrically poled prior to ME measurements to increase its ferroelectric response. It is well-known that when the PFM tip contact the sample surface for measurements, it exerts a compressive stress of ~100 MPa[44]. This stress is large enough to induce strains in the local piezo/ferro electric domains, which has an effect on the measured ME coefficient. Similarly, Deng *et al.*[42] used hydrothermal reaction and polymer assisted deposition to fabricate single crystal $CoFe_2O_4$ nanorods embedded in $BaTiO_3$ matrix and obtained a ME coefficient of 51 $mV.cm^{-1}.Oe^{-1}$. This quite high ME coefficient value obtained is attributed to the large interfacial area induced by the nano-sized $CoFe_2O_4$ and $BaTiO_3$ phases and 'perfect interface' achieved by using polymer assisted deposition. It should be noted that multi-layered $BaTiO_3/CoFe_2O_4$ composites[45] give the lowest ME coefficient value.

It is well-known that the ME effect in composites is a product tensor property and is typically affected by (i) the geometry and morphology of the phases, (ii) interfacial bonding between the phases, (iii) individual properties of each constituent phase, and (iv) thickness and number of magnetostrictive and ferroelectric phases[2,3,5]. In our work, we believe the increased ME coefficient is a direct result of the unique electrospinning process. Electrospinning followed by thermal annealing of precursor fibers leads to the formation of composite fibers composed of $BaTiO_3$ and $CoFe_2O_4$ grains. The grain sizes of individual phases are in the range of tens of nanometers. Nanoscale sizes of these grains can induce large interfacial area, which will favour elastic interactions between the ferroelectric and ferromagnetic phases. It is also known that large interfacial area and good phase connectivity play a role in contributing to the strong ME effect. Moreover, it is clear from the TEM images in Figure 2 that the obtained fibers have $BaTiO_3$ and $CoFe_2O_4$ in close proximity. This ensures that the phases are tightly bound and the strains can be readily transferred to the neighboring grains. Hence, the phase -connectivity of these nanostructures also contributes towards the ME effect of the composite.

Further increase in magnitude of the magnetic field beyond the critical value of 1810 Oe leads to decreasing ME coefficient values. Ferromagnetic materials can change their shape during the process of magnetization and this property is called magnetostriction. As the magnetic field is increased, the magneto -striction increases gradually and attains a maximum value. During this stage, the strain produced in the ferromagnetic material is transferred to the ferroelectric $BaTiO_3$ phase due to the coupling between the ferromagnetic and ferroelectric phases. The ferroelectric phase produces a voltage in response to the strain. Beyond ~1810 Oe, the magnetostriction and the strain produced in the composite would produce a constant electric field in the ferroelectric phase. Beyond saturation magnetization, the magnetostriction and the strain thus produced in the $CoFe_2O_4$ phase generates a constant electric field in the piezoelectric $BaTiO_3$ phase [39]. This suggests that change of electric field (*dE*) per applied magnetic field change (*dH*), *dE/dH*, which is a measure of magnetoelectric coefficient decreases as the magnetic field is increased beyond the critical value of ~1810 Oe. Thus, the magnetostrictive coefficient reaches saturation at ~1810 Oe. This explains why the ME coefficient increases initially and then begins to decrease when the applied magnetic field is increased beyond a critical value. This trend in the ME coefficient *versus* magnetic field can be attributed to the spinel ferrite phase of $CoFe_2O_4$ [10, 11, 39].

Table 1 ME coefficient and saturation magnetization values of $CoFe_2O_4/BaTiO_3$ composites

No	Composite morphology	$CoFe_2O_4$: $BaTiO_3$ ratio	Characteristic size	M_s (emu/g)	ME coefficient ($mV.cm^{-1}.Oe^{-1}$)	Ref
1	Fibers	1:1	140 nm	31	13.3 at ~2 kOe	This study
2	Core-shell powder	-	10 nm	72	3.4 at 1 kOe	[11]
3	Core-shell powder	-	10 nm	72	2 at 1 kOe	[10]
4	Powder	1:4	-	16	0.43 at ~ 5.2 kOe	[36]
		2:3	-	30	0.375 at ~ 5.7 kOe	
5	Core-shell powder	2:10	40 nm	-	0.3	[38]
		3:10			0.48	
		4:10			1	
		5:10			1.47	
		6:10			0.42	
6	Multi-layered composite	-	$CoFe_2O_4$- 150 nm; $BaTiO_3$-100 nm	~90	0.036 at 2.8k Oe	[45]
7	Powder	1:1	50-80 nm	37.5	17.04 at 2 kOe	[41]
8	Nano-lamellar bi-crystals	1:1	-	-	20 at 10 Oe	[40]
9	Feather-like nanostructures	-	Diameter - 250 nm; length - 5 μm	20	51 at 3 kOe	[42]
10	$CoFe_2O_4$ nanorods embedded in $BaTiO_3$ matrix	7:13	Thickness -400 nm	~400 (emu/cm^3)	1.2 x 10^3	[43]

Conclusion

In summary, our results demonstrate that the $BaTiO_3/CoFe_2O_4$ fibers obtained by electrospinning possess excellent ferro-magnetic and ME properties. The ME coefficient of these one-dimensional structures are found to be much higher than their bulk or thin film counterparts. The large value of the ME coefficient is attributed to the electrospinning technique which produces fibers with diameters in the range of 100-200 nm. The $BaTiO_3$ and $CoFe_2O_4$ grains within the fibers display sizes of few tens of nanometers. Consequently, they provide large interfacial areas and excellent interphase connectivity so that the composite fibers have large ME coefficients. These one-dimensional electrospun composite fibers show tremendous potential as novel ME materials for nanoscale devices and applications.

Acknowledgement

We thank the Australian Research Council (ARC) for the continuous support of this project (#DP0665856). AB is Research Associate funded by the ARC.

Notes and references

[a] *Centre for Advanced Materials Technology (CAMT), School of Aerospace, Mechanical and Mechatronic Engineering J07, The University of Sydney, Sydney, Australia*
[b] *Engineering Product Development (EPD) Pillar, Singapore University of Technology and Design (SUTD), Singapore, Singapore. Fax: 65 6779 5161; Tel: 65 6499 4502; E-mail: avinash_baji@sutd.edu.sg*
[c] *School of Physics, Institute of Science, Suranaree University of Technology, Nakhon Ratchasima, Thailand*
[d] *Department of Materials Engineering, Faculty of Engineering and Architecture, Rajamangala University of Technology Isan, Nakhon Ratchasima, Thailand*

1. C. W. Nan, *Phys. Rev. B*, 1994, **50**, 6082.
2. C. W. Nan, M. I. Bichurin, S. X. Dong, D. Viehland and G. Srinivasan, *J. Appl. Phys.*, 2008, **103**, 031101.
3. G. Srinivasan, in *Annual Review of Materials Research, Vol 40*, eds. D. R. Clarke, M. Ruhle and F. Zok, Annual Reviews, Palo Alto, Editon edn., 2010, vol. 40, pp. 153-178.
4. A. Baji, Y-W. Mai, Q. Li and Y. Liu, *Compos. Sci. Technol.*, 2011, **71**, 1435.

5. W. Eerenstein, N. D. Mathur and J. F. Scott, *Nature*, 2006, **442**, 759.
6. A. Baji, Y-W. Mai, Q. A. Li, S. C. Wong, Y. Liu and Q. W. Yao, *Nanotechnology*, 2011, **22**, 235702.
7. A. Baji, Y-W. Mai, Q. Li and Y. Liu, *Nanoscale*, 2011, **3**, 3068.
8. T. Lottermoser, T. Lonkai, U. Amann, D. Hohlwein, J. Ihringer and M. Fiebig, *Nature*, 2004, **430**, 541.
9. J. Ryu, S. Priya, K. Uchino and H. E. Kim, *J. Electroceram.*, 2002, **8**, 107.
10. G. V. Duong, R. Groessinger and R. S. Turtelli, *IEEE Trans. Magn.*, 2006, **42**, 3611.
11. G. V. Duong and R. Groessinger, *J. Magn. Magn. Mater.*, 2007, **316**, E624.
12. J. Y. Zhai, N. Cai, Z. Shi, Y. H. Lin and C. W. Nan, *J. Phys. D-Appl. Phys.*, 2004, **37**, 823.
13. S. Y. Tan, S. R. Shannigrahi, S. H. Tan and F. E. H. Tay, *J. Appl. Phys.*, 2008, **103**, 094105.
14. S. Chandarak, S. Pojprapai, S. Srilomsak, P. Jantaratana, S. Rujirawat and R. Yimnirun, *Ferroelectrics*, 2011, **419**, 70.
15. H. Zheng, J. Wang, S. E. Lofland, Z. Ma, L. Mohaddes-Ardabili, T. Zhao, L. Salamanca-Riba, S. R. Shinde, S. B. Ogale, F. Bai, D. Viehland, Y. Jia, D. G. Schlom, M. Wuttig, A. Roytburd and R. Ramesh, *Science*, 2004, **303**, 661.
16. C. W. Nan, G. Liu, Y. H. Lin and H. D. Chen, *Phys. Rev. Lett.*, 2005, **94**, 197203.
17. D. A. Pan, Y. Bai, W. Y. Chu and L. J. Qiao, *J. Phys. D-Appl. Phys.*, 2008, **41**, 022002.
18. S. Agrawal, J. P. Cheng, R. Y. Guo, A. S. Bhalla, R. A. Islam and S. Priya, *Mater. Lett.*, 2009, **63**, 2198.
19. V. M. Petrov, G. Srinivasan, U. Laletsin, M. I. Bichurin, D. S. Tuskov and N. Paddubnaya, *Phys. Rev. B*, 2007, **75**, 174422.
20. M. Kumar and K. L. Yadav, *Mater. Lett.*, 2007, **61**, 2089.
21. J. Xiang, X. Q. Shen, F. Z. Song and M. Q. Liu, *J. Solid State Chem.*, 2010, **183**, 1239.
22. S. H. Xie, J. Y. Li, Y. Y. Liu, L. N. Lan, G. Jin and Y. C. Zhou, *J. Appl. Phys.*, 2008, **104**, 024115.
23. B. Liu, T. Sun, J. Q. He and V. P. Dravid, *ACS Nano*, 2010, **4**, 6836.
24. K. Prashanthi, P. M. Shaibani, A. Sohrabi, T. S. Natarajan and T. Thundat, *Phys. Status Solidi-Rapid Res. Lett.*, 2012, **6**, 244.
25. S. H. Xie, F. Y. Ma, Y. M. Liu and J. Y. Li, *Nanoscale*, 2011, **3**, 3152.
26. Q. Zhu, Y. Xie, J. Zhang, Y. Liu, Q. Zhan, H. Miao and S. Xie, *J. Mater. Res.*, 2014, **29**, 657.
27. L. Zhang, J. W. Zhai, W. F. Mo and X. Yao, *Ferroelectrics*, 2010, **406**, 213.
28. K. Raidongia, A. Nag, A. Sundaresan and C. N. R. Rao, *Appl. Phys. Lett.*, 2010, **97**, 3478231.
29. S. Rizwan, S. Zhang, Y. G. Zhao and X. F. Han, *Appl. Phys. Lett.*, 2012, **101**, 082414.
30. S. Zhang, Y. G. Zhao, P. S. Li, J. J. Yang, S. Rizwan, J. X. Zhang, J. Seidel, T. L. Qu, Y. J. Yang, Z. L. Luo, Q. He, T. Zou, Q. P. Chen, J. W. Wang, L. F. Yang, Y. Sun, Y. Z. Wu, X. Xiao, X. F. Jin, J. Huang, C. Gao, X. F. Han and R. Ramesh, *Phys. Rev. Lett.*, 2012, **108**, 137203.
31. R. S. Devan, D. R. Dhakras, T. G. Vichare, A. S. Joshi, S. R. Jigajeni, Y.-R. Ma and B. K. Chougule, *J. Phys. D-Appl. Phys.*, 2008, **41**, 105010.
32. N. Z. Bao, L. M. Shen, Y. H. Wang, P. Padhan and A. Gupta, *J. Am. Chem. Soc.*, 2007, **129**, 12374.
33. M. Arias, V. M. Pantojas, O. Perales and W. Otano, *J. Magn. Magn. Mater.*, 2011, **323**, 2109.
34. I. S. Jacobs and C. P. Bean, *Phys. Rev.*, 1955, **100**, 1060-1067.
35. D. Li, T. Herricks and Y. N. Xia, *Appl. Phys. Lett.*, 2003, **83**, 4586.
36. L. M. Hrib and O. F. Caltun, *J. Alloy. Compd.*, 2011, **509**, 6644.
37. M. B. Kothale, K. K. Patankar, S. L. Kadam, V. L. Mathe, A. V. Rao and B. K. Chougule, *Mater. Chem. Phys.*, 2003, **77**, 691.
38. V. Corral-Flores, D. Bueno-Baques, D. Carrillo-Flores and J. A. Matutes-Aquino, *J. Appl. Phys.*, 2006, **99**, 08j503.
39. A. Hanumaiah, T. Bhimasankaram, S. V. Suryanarayana and G. S. Kumar, *Bull. Mat. Sci.*, 1994, **17**, 405.
40. S. Ren, M. Laver and M. Wuttig, *Appl. Phys. Lett.*, 2009, **95**, 153504.
41. J. Nie, G. Xu, Y. Yang and C. Cheng, *Mater. Chem. Phys.*, 2009, **115**, 400.
42. Y. Deng, J. Zhou, D. Wu, Y. Du, M. Zhang, D. Wang, H. Yu, S. Tang and Y. Du, *Chem. Phys. Lett.*, 2010, **496**, 301.
43. F. Bai, H. Zhang, J. Li and D. Viehland, *J. Phys. D-Appl. Phys.*, 2010, **43**, 285002.
44. A. Gruverman, A. Kholkin, A. Kingon and H. Tokumoto, *Appl. Phys. Lett.*, 2001, **78**, 2751.
45. D. Zhou, L. Hao, S. Gong, Q. Fu, F. Xue and G. Jian, *J. Mater. Sci.-Mater. El.*, 2012, **23**, 2098.